Chitin-Incorporated Poly(ethylene oxide)-Based Nanocomposite Electrolytes for Lithium Batteries

A. Manuel Stephan,*,† T. Prem Kumar,† M. Anbu Kulandainathan,‡ and N. Angu Lakshmi†

Electrochemical Power Systems and Electro-Organic Divisions, Central Electrochemical Research Institute, Karaikudi 630 006, India

Received: June 30, 2008; Revised Manuscript Received: December 3, 2008

Nanocomposite polymer electrolytes (NCPE), with different proportions of poly(ethylene oxide)/$LiClO_4$/chitin were prepared by a hot press method. Nanochitin, a biopolymer, poly(β-(1→4)-*N* acetyl-D-glucosamine) was incorporated as a filler in poly(ethylene oxide) (PEO). The ionic conductivity of the composite polymer electrolytes was enhanced by one order upon addition of nanochitin. The lithium transference number, t_{Li}^+, was increased from 0.24 to 0.51 upon chitin addition. The membranes were subjected to scanning electron microscopy, thermogravimetric−differential thermal analysis, differential scanning calorimetry, ionic conductivity, and Fourier transform infrared (FTIR) spectroscopy analysis. The free volume V_f was probed by positron annihilation lifetime spectroscopy studies at 30 °C. Li/NCPE/Li symmetric cells were assembled, and the thickness of the solid electrolyte interface as a function of time was analyzed. This paper also describes FTIR spectroscopic studies of the interface between lithium metal and NCPE, which suggests that the surface chemistry of lithium electrodes in contact with NCPE is dominated by compounds with C−N−Li and C−O−Li bonding.

1. Introduction

Rechargeable lithium batteries have become the sources of choice not only for portable electronic devices (laptop computers, mobile phone etc.) but also for hybrid electric vehicle applications.[1−3] Commercially available lithium-ion cells employ a lithium-intercalating polycrystalline oxide as the cathode and a carbon anode with a nonaqueous liquid electrolyte. The liquid electrolyte is a cause for concern, and its flammability during inadvertent cell abuse can lead to safety hazards.[4] However, this problem can be circumvented by replacing liquid electrolytes with solid polymer electrolytes.

Advantages such as nonleakage of electrolyte, high energy density, flexible geometry, and improved safety characteristics have led to an unprecedented interest in the development of polymer electrolytes for lithium batteries. Polymer electrolytes can be broadly classified into three types: (i) dry, (ii) gel, and (iii) composite polymer electrolytes. The ionic conductivity of dry polymer electrolytes can reach reasonably high values (i.e., on the order of 10^{-4} S cm^{-1}) only at temperatures above 90 °C.[5] In the last two decades numerous attempts have been made to improve the ionic conductivity at ambient and subambient temperatures.[6,7] One of the best approaches involves addition of low molecular weight plasticizers such as ethylene carbonate, propylene carbonate, etc. to the polymer matrix.[8] Although, addition of plasticizers enhances the ionic conduction of the system significantly, the mechanical robustness of membranes is adversely affected.

Further more, the plasticizers react with the lithium metal anode and deteriorates its surface, resulting in serious problems regarding battery cyclability and safety. Recent studies reveal that only ceramic/inert filler (ZrO_2, SiO_2, Al_2O_3) -incorporated composite polymer electrolytes can offer safe and reliable batteries.[9,10] The concept of incorporating inert fillers into the polymer−LiX salt complexes is not new. This procedure has already been adopted successfully to enhance the mechanical stability (brought about by a network of filler particles in the polymer matrix), improve compatibility of solid polymer electrolytes with lithium metal anode, as well as to achieve high ionic conductivity.[10] Polymer hosts investigated so far include poly(ethylene oxide) (PEO), poly(propylene oxide) (PPO), poly(acrylonitrile) (PAN), poly(methyl methacrylate) (PMMA), poly(vinyl chloride) (PVC), poly(vinylidene fluoride) (PVdF) and poly(vinylidene fluoride-hexafluoro propylene) (PVdF-HFP).[11−13] Poly (ethylene oxide) as a host has been most extensively studied for battery applications.

PEO chains adopt a helical conformation with all the C−O bonds in trans and the C−C bonds in either gauche or gauche minus configuration.[14] In this geometry, cations can be located in each turn of the helix and are coordinated by three ether oxygens. However, the basic structure of the host is retained for all sizes of anions. In the present study, chitin was employed as inert filler for the first time. Chitin, poly(β-(1→4)-*N*-acetyl-D-glucosamine), is the most abundant biopolymer after cellulose.[15] Chitin occurs as ordered crystalline microfibrils and is useful in applications that require reinforcement and strength. Chitin is available in two allomorphs, namely, α and β forms, which can be differentiated by infrared, solid-state nuclear magnetic resonance (NMR), and X-ray diffraction (XRD) spectroscopies.[16] Chitin has low toxicity and is biodegradable and antibacterial. It also possesses gel-forming properties and finds applications not only in the food industry, but also in biosensors.[17] To the best of our knowledge, chitin has never before been investigated as filler in nanocomposite polymer electrolytes for battery applications. Recent studies indicate that membranes prepared by conventional solvent casting method lead to poor interfacial properties at the lithium/polymer electrolyte interface.[18] Impurities, mostly the traces of solvent,

* Corresponding author e-mail: amanstephan@yahoo.com; fax: +91 4565 227779.
† Electrochemical Power Systems Division.
‡ Electro-Organic Division.

10.1021/jp808640j CCC: $40.75
Published on Web 01/22/2009

TABLE 1: The Composition of Polymer, Chitin, and Lithium Salt

sample	polymer (wt %)	chitin (wt %)	$LiClO_4$ (wt %)
S1	95	0	5
S2	90	5	5
S3	85	10	5
S4	75	17	8
S5	70	20	10
S6	94	5	1
S7	93	5	2
S8	92	5	3
S9	91	5	4

are trapped in the high surface area, nanosized inert fillers in solvent-cast electrolytes, even after prolonged drying.[18] Hence, in the present study the hot press technique was employed for the preparation of nanocomposite polymer electrolytes.

2. Experimental Procedure

2.1. Synthesis of Nanochitin. The chitin precursor was purchased from local sources in India and was boiled and stirred with a 5% aqueous solution of KOH for 6 h in order to remove most of the proteins. Subsequently, it was washed with distilled water and dried. This process was repeated three times. The sample was then bleached with 17 g of NaCl in 1 L of water containing 0.3 M sodium acetate buffer for 6 h at 80 °C. The bleaching solution was changed every 2 h. The chitin suspension was then kept in 5% KOH for 72 h to remove any residual protein, centrifuged at 3000 rpm/min for 20 min, and hydrolyzed with 3 N HCl under stirring for 1.5 h. After hydrolysis, the suspension was transferred to a dialysis bag and dialyzed for 24 h until its pH reached a value of 6. The pH of the suspension was adjusted to 3.5 with HCl. The dispersed whiskers were treated ultrasonically and were filtered to remove residual aggregates. The resulting nanochitin was preserved in a refrigerator with sodium azoture as a protectant against microorganisms.

2.2. Preparation of Nanocomposite Polymer Electrolytes. PEO (Aldrich) and lithium perchlorate, $LiClO_4$ (Merck), were dried under vacuum for 2 days at 50 and 100 °C, respectively. Nanochitin was also dried under vacuum at 50 °C for 5 days before use. Nanocomposite polymer electrolytes were prepared by dispersing appropriate amounts of chitin in PEO - $LiClO_4$ (Table 1) and hot-pressing into films as described elsewhere.[18,19] The nanocomposite electrolyte films had an average thickness of 30−50 μm. This procedure yielded homogeneous and mechanically strong membranes, which were dried under vacuum at 50 °C for 24 h for further characterization.

2.3. Electrochemical Characterization. The ionic conductivity of the membranes sandwiched between two stainless steel blocking electrodes (1 cm^2 diameter) was measured using an electrochemical impedance analyzer (IM6-Bio Analytical Systems) in the 50 mHz to 100 kHz frequency range at various temperatures (0, 15, 30, 40, 50, 60, 70, and 80 °C). Symmetric nonblocking cells of the type Li/NCPE/Li were assembled for compatibility, which was investigated by studying the time-dependence of the impedance of the systems under open-circuit potential at 80 °C.

The lithium transference number was calculated by the method proposed by Vincent and co-workers.[20] The following formula was adopted to measure the lithium transference number.[7,21]

$$t_{Li}^{+} = \frac{I_{ss}(V - I_0R_0)}{I_o(V - I_sR_{ss})} \quad (1)$$

The Li/NCPE/Li cell was polarized by a dc pulse of 10 mv. Time evolution of the resulting current flow was then followed. The initial (I_0) and steady state (I_{ss}) values of current flowing through the cell during the polarization were measured. R_0 and R_{ss} represent the resistance values before and after the perturbation of the system. Impedance spectra were made before and after the pulse application in order to correct the changes.

Morphological examination of the films was made by a scanning electron microscope (FE-SEM, S-4700, Hitachi) under a vacuum condition (10^{-1} Pa) after sputtering gold on one side of the films. Differential scanning calorimetry (DSC) measurements were performed at a rate of 10 °C min^{-1} between 20 and 250 °C, and in TG-DTA the temperature range was 20−300 °C. The lithium/ polymer electrolyte interface was analyzed using Fourier transform infrared spectroscopy (FTIR, Thermo NICOLET Corporation, Nexus Model −670) by single internal reflection (SIR) mode.[22] The infrared spectra were obtained at ambient temperature with an 8 cm^{-1} resolution. Positron annihilation lifetime spectroscopy (PALS) measurements were made using a ^{22}Na source (ORTEC) with a resolution of 250 ps. The data were collected at 30 °C on a 70 μm thick nanocomposite polymer membrane, and the spectrum was analyzed by the PATFIR-88 program.

3. Results and Discussions

3.1. Ionic Conductivity. Panels a and b in Figure 1 are the plots of conductivity as a function of the reciprocal of the temperature for different concentrations of $LiClO_4$ and chitin, respectively. To highlight the influence of chitin on ionic conductivity, a plot for filler-free sample is also given. The results presented are averages of two cells for each NCPE sample. It is seen from Figure 1a that the ionic conductivity increases with increase in temperature and salt concentration. All the curves (Figure 1a) show a slow and continuous change in the slope up to around 60 °C, beyond which there is a remarkable change in slope, reflecting the well-known transition from the crystalline to the amorphous phase of PEO. This transition contributes to an increase in ionic conductivity. These results are in accordance with those reported on PEO-based polymer electrolytes with lithium imide anions.[23−25] Figure 1b clearly illustrates that incorporation of nanochitin fillers enhanced the ionic conductivity up to one order of magnitude. The corresponding Nyquist plots are shown in the inset.

According to Wieckzorek et al.,[26,27] the Lewis base reactions between the filler surface and the PEO segments may induce structural modifications in the polymer matrix. The Lewis acid character of the added ceramics (γ-Al_2O_3) would compete with the Lewis acid character of lithium cations for the formation of complexes with the PEO chains. In the present study, chitin would act as cross-linking centers for the PEO segments, which lowers the polymer chain reorganization tendency, thus promoting an overall stiffness to the structure. However, the resulting structure provides Li^+-conducting pathways at the filler surface and enhances ionic transport.[27]

3.2. Lithium Transference Number. Although high ionic conductivity, enhanced thermal stability, and good compatibility with lithium electrodes are desirable properties, they are not sufficient enough to make a membrane useful for practical applications. The fraction of the current carried by Li^+ ions through the polymer electrolyte is determined in the performance

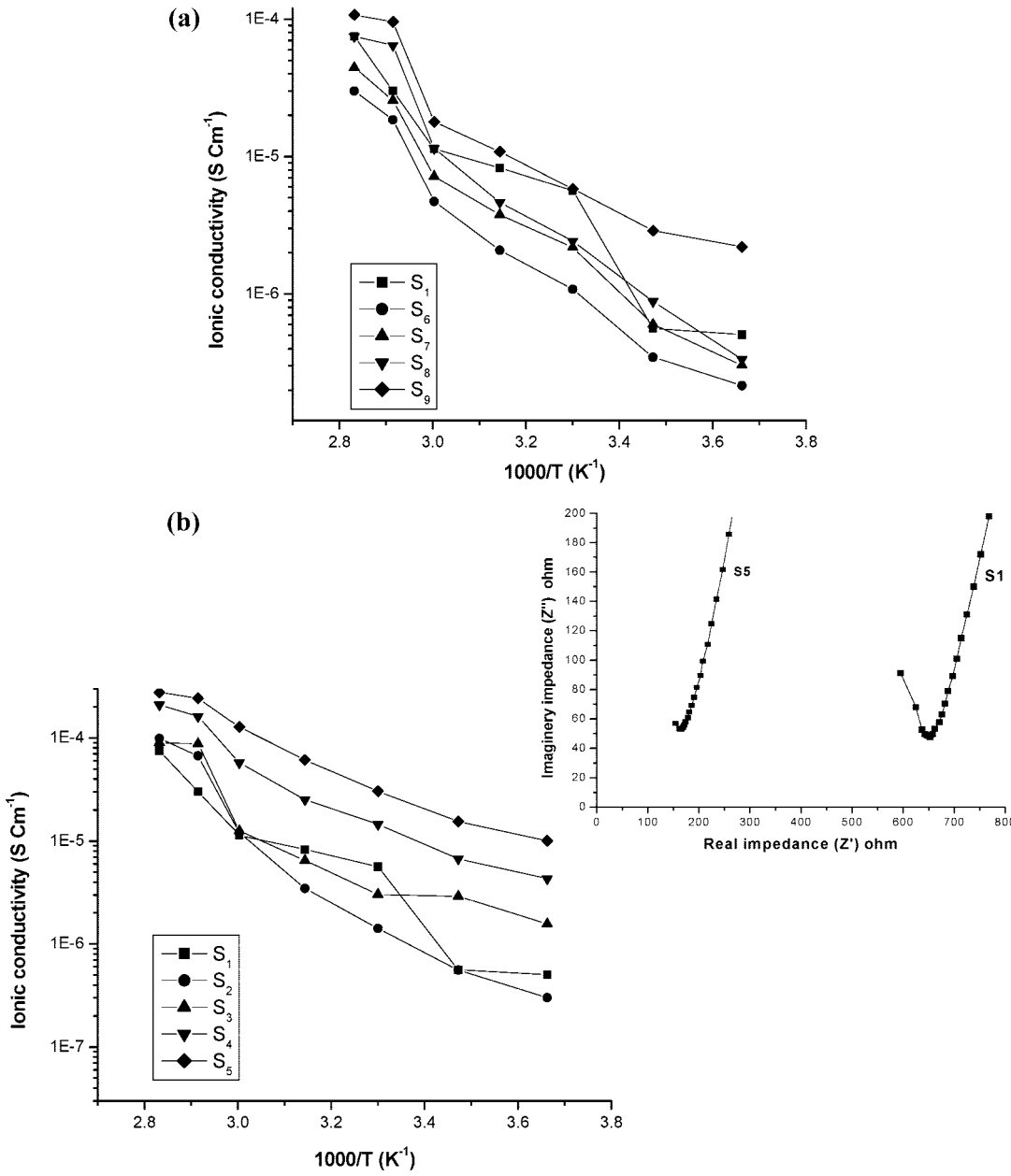

Figure 1. (a) Ionic conductivity as a function of temperature for different concentrations of $LiClO_4$. (b) Ionic conductivity as a function of temperature for different lithium salt concentrations. Inset: Nyquist plot of samples S1 and S5 at 30 °C.

of lithium batteries. The effective cationic conductivity is generally expressed by the relation

$$\sigma_{Li}^{+} = t_{Li}^{+}\sigma_{Total} \quad (2)$$

where σ_{Total} is the total conductivity.[18] To understand the effectiveness of chitin in enhancing ionic conductivity the transference number studies were carried out on samples S1 and S5 at 80 °C, a temperature that is found to be optimal from a conductivity point of view for practical applications. The Li^+ transference numbers for samples S1 and S5 were found to be 0.24 and 0.50, respectively. According to Capiglia et al.,[24] who reported the transference numbers in the $P(EO)_{20}$-LiBETI-SiO_2 system, increase in transference number for Li^+ ions was due to moisture trapped in the nanoparticles of SiO_2. In the present study, since the NCPE were prepared by a hot press technique with dry constituents, the increase in transference number may be attributed to increased salt dissociation due to the formation of ion−chitin complexes by Lewis acid−base interactions between the surface groups of the chitin and anions.[28]

3.3. Interfacial Properties of Li/NCPE/Li Cells. Lithium is an attractive anode metal with a theoretical capacity of 3862 mA h g^{-1}. However, its cyclability is limited by dentritic deposition upon recharge. Moreover, lithium is lost in every cycle due to the formation of a solid electrolyte interphase (SEI) with the electrolyte. Thus, the interfacial properties of lithium metal anodes in contact with the electrolyte are critical in practical applications. Numerous studies have been made on the charge−discharge characteristics of lithium anode.[29−31] However, only a few studies have been devoted to the interface properties of lithium and lithiated carbon electrodes in contact with solid polymer electrolytes. Specifically, there is hardly any report on this structure of the interphase between lithium metal and NCPE. Infrared spectroscopic measurements provide information on the surface chemistry of lithium metal (chemical

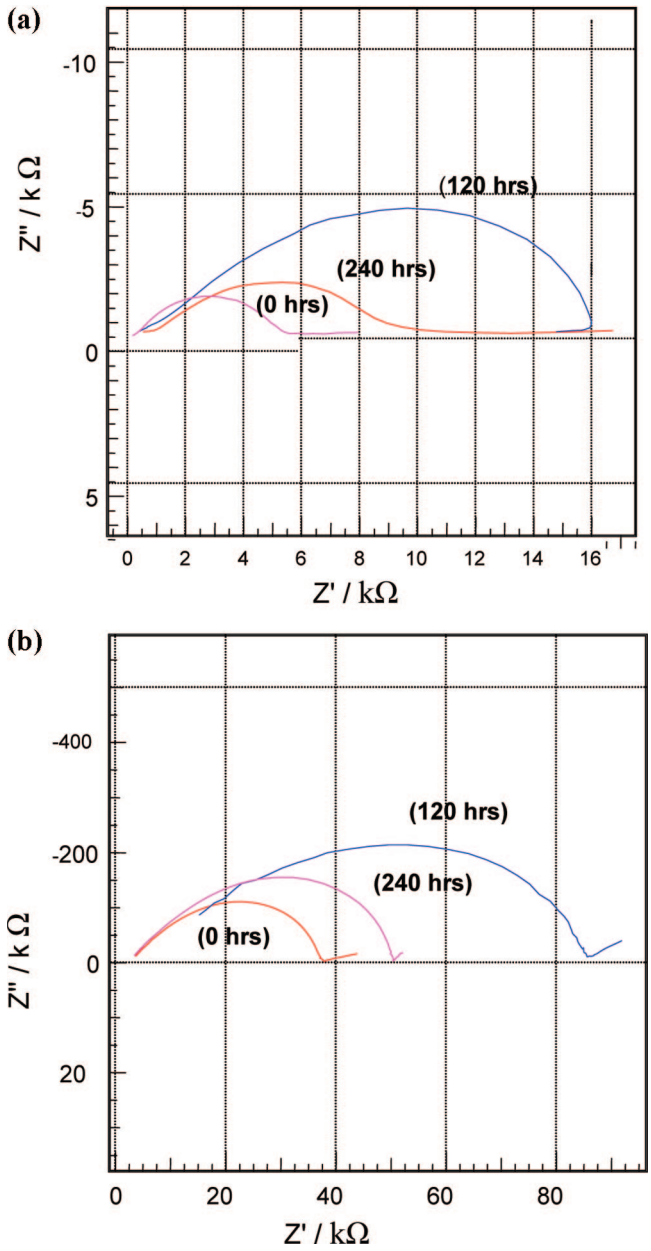

Figure 2. (a)Selected impedance spectra of Li/PEO + $LiClO_4$/Li cells at 80 °C under open-circuit condition. (b) Selected impedance spectra of Li/PEO + chitin + $LiClO_4$/Li cells at 80 °C under open circuit condition.

composition) upon contact with polymer electrolyte. The solid polymer electrolyte−lithium interface plays a vital role in the electrochemical behavior of the lithium−polymer cells.[32] Major techniques for studying the interface are FTIR, XPS, and energy dispersive x-ray analysis (EDAX). Techniques such as AES and Raman spectroscopy may also be useful, although they may be destructive to the lithium metal surface.[33,34]

Panels a and b in Figure 2 show the Cole−Cole impedance spectra of Li/NCPE/Li with chitin-free and chitin-added membranes for different storage times at 80 °C under open-circuit conditions. In the present study, sample S5 was employed, as it exhibited the maximum ionic conductivity. The shape of the impedance response is similar for both the polymer electrolytes. Figure 3 shows the variation of interfacial resistance as a function of time of the Li/NCPE/Li symmetric cells at 80 °C. It is clear from the figure that the interfacial resistance of chitin-added sample is substantially lower than that of the filler-free

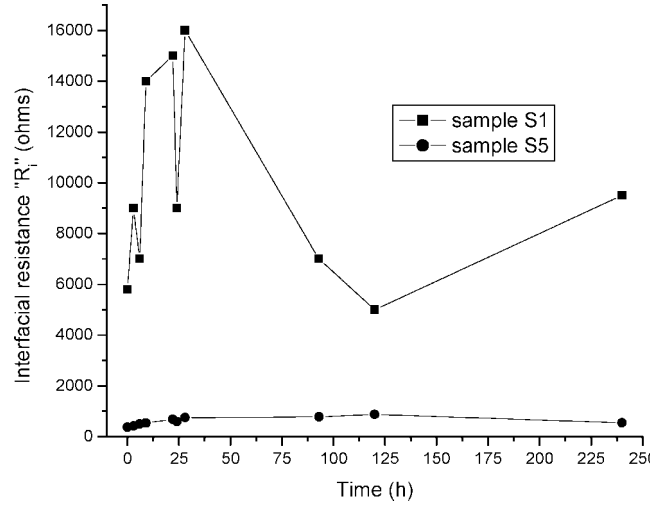

Figure 3. Interfacial resistance as a function of time for the sample S1 (without chitin) and S5 (with chitin).

sample. Furthermore, the interfacial resistance remained stable over long periods of storage (240 h).

The thickness of the SEI was measured using the relationship[35]

$$t = 2\pi f_{max}\varepsilon_0\varepsilon_r A R_i \quad (3)$$

where A is the area of the electrode surface, R_i the interfacial resistance, f_{max} is the frequency maximum, and ε_0 and ε_r correspond to the permittivity of air and the lithium material, respectively. The value of ε_r for lithium-based materials is taken as 10.[35] In the present study the average thickness of the SEI was calculated to be on the order of 5−10 Å for both membranes with and without chitin. According to Aurbach et al.,[22] the interfacial resistance of Li electrodes developed during storage time is primarily due to differences in the resistivity of the films formed rather than due to differences in their thickness. The thickness of the SEI layers in the present study is comparable to that of plasticized PEO/$LiClO_4$ complexes.[36]

Figure 4a shows the FTIR spectrum of nanocomposite electrolyte comprising PEO + $LiClO_4$ + chitin (sample S5). The FTIR spectra obtained with a lithium electrode in contact with PEO + $LiClO_4$ and PEO + chitin + $LiClO_4$ polymer membranes (through KBr window) at room temperature are shown in panels b and c in Figure 4. In the spectra shown in panels b and c of Figure 4, the original features belonging to the polymer electrolytes not only disappeared, but new peaks have arisen. In Figure 4b the peak that appears at 3670 cm^{-1} is attributed to a −OH group. On the other hand, when a chitin-incorporated composite electrolyte comes into contact with the lithium metal anode, new peaks appear at 1077 and 1204 cm^{-1}. The peak that appears at 1077 cm^{-1} is attributed to −C−O−Li, whereas the one at 1204 cm^{-1} is due to −C−N−Li.[37] Moreover, the peaks appearing between 1400 and 1455 cm^{-1} are attributed to −C═O and $-CH_2{=}CH_3$.[35] It is significant that in the present study no predominant peak that normally appears around 1100 cm^{-1} and is attributable to the reduction of $LiClO_4$ to $LiClO_y$ species is present.[22]

According to Shin and co-workers,[18] commercially available PEO contains about 1 wt % of calcium compounds originating from the neutralization of the catalyst used in its synthesis. The CaO particles are very small and are intimately mixed with the PEO. PEO also contain up to 3 wt % of fumed silica, which is used to modify the fluidity of the polymer powder during

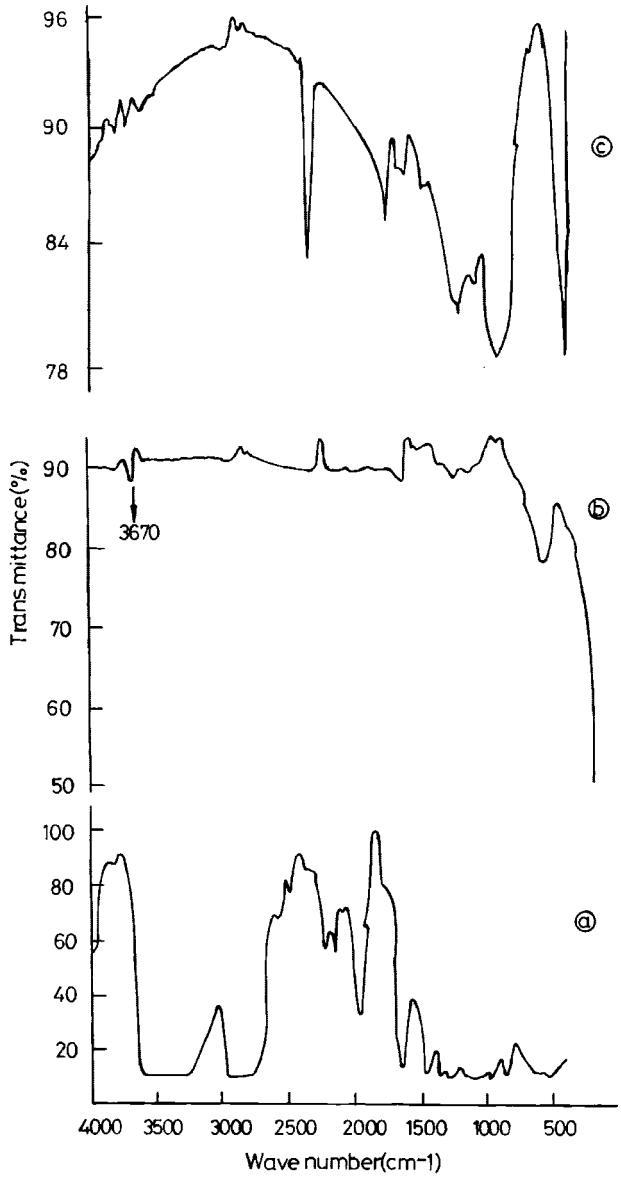

Figure 4. FTIR spectra of (a) sample S2 and (b) sample S1, and (c) in situ FTIR of the lithium surface.

synthesis. Furthermore, these constituents may react with lithium and lead to the formation of new compounds on the metal surface.

3.4. FT-IR Analysis. Being sensitive to molecular and structural changes in the polymer electrolyte systems, FT-IR has been identified as a powerful tool to study the complexation between salts and polymers. Traces a−d in Figure 5 show, respectively, the IR spectra of PEO, chitin, PEO + $LiClO_4$, and PEO + chitin + $LiClO_4$. The band in Figure 5a that appears at 2886 cm^{-1} can be assigned to the −C−H stretching mode, and the peak at 1967 cm^{-1} is due to an asymmetric stretching mode. The peaks at 1466, 1103, 956, and 841 cm^{-1} are assigned to $-CH_2-$ scissoring, −C−O−C− stretching, $-CH_2$ twisting, and $-CH_2-$ wagging modes, respectively.[36−38] Also, PEO exhibits −C−H stretching (between 2800 and 2935 cm^{-1}), asymmetric stretching (1950−1970 cm^{-1}), asymmetric bending (1450 cm^{-1}), CH_2 scissoring (1465−1485 cm^{-1}), C−O−O stretching (1250−950 cm^{-1}), $-CH_2-$ twisting (991 cm^{-1}), and $-CH_2-$ wagging (842 cm^{-1}).[39,40]

Several IR spectral studies have been made on the infrared spectra of chitin.[41,42] Because of the high crystallinity of the

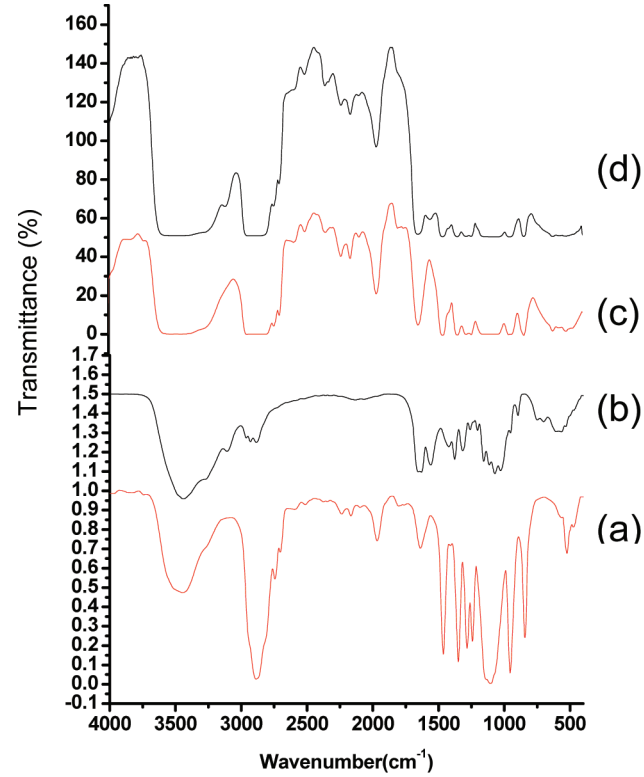

Figure 5. FTIR spectra of (a) PEO, (b) chitin, (c) PEO + LiClO4, and (d) PEO + chitin + LiClO4.

sample (Figure 5b), it displays a series of very sharp absorption bands. For example, the peak at 1560 cm^{-1} is characteristic of an amide II group. The band at 1638 cm^{-1} is assigned to a −C═O group hydrogen-bonded to −N−H of the neighboring intrasheet chain in chitin. Upon incorporation of $LiClO_4$ in the polymer host, the peak at 956 cm^{-1} shifts to 961 cm^{-1}. In a similar way, the characteristic frequencies of $LiClO_4$ at 1300 and 920 cm^{-1} are shifted, respectively, to 1350 and 940 cm^{-1} (Figure 5c). The shifts in their corresponding characteristic frequencies are attributed to changes in the environment of $-ClO_4^-$. Similarly, with incorporation of chitin in the PEO matrix (Figure 5d), the intensity of the peak is significantly reduced and is even slightly shifted to 1557 cm^{-1}, which indicate formation of a complex in the system. These results are in accordance with Ramesh et al.,[43] who reported the interactions of different lithium salts with the PEO matrix.

3.5. Positron Annihilation Lifetime Spectroscopy Studies. The local free volumes of polymers, or in other words the cavities or holes of atomic and molecular dimensions, arise in polymers because of irregular molecular packing in the amorphous phase (static and pre-existing holes), and molecular relaxation of the polymer chains and terminal ends with low electron density.[44,45] The holes can lower the density of the amorphous phase by as much as 10% as compared to the density of the crystalline phase of the same polymeric material. Hence, free volume plays a vital role in the thermal, mechanical, and relaxation properties of polymer. The free volume is generally defined as

$$V_f = V_t - V_0 \quad (4)$$

where V_t is the total volume, and V_0 is the volume occupied by the molecules. Techniques such as positron annihilation lifetime spectroscopy, small-angle X-ray scattering (SAXS), neutron

diffraction, photochromic, and fluorescence spectroscopy are widely used to measure the free volume of polymer samples. The scanning tunneling microscopy (STM), atomic force microscopy (AFM), scanning electron microscopy (SEM), and transmission electron microscopy (TEM) have also been employed for this purpose. However, diffraction method is very difficult for hole sizes below 10 Å. Moreover, selected size probes should be introduced into the holes in the photochromic and fluorescence methods, which may damage the membrane. STM, SEM, TEM, and AFM are more sensitive to static holes (10 Å or larger) present on the surface. On the other hand, positron annihilation lifetime spectroscopy has drawn the attention of many researchers in recent years due to its sensitivity, specialty, and amenability to in situ measurements.

According to the free volume model,[44,46−49] in the absence of any positron and/or positronium interactions, inhibition of Ps formation and quenching of ortho-positronium lifetime affect the parameters τ_3 and I_3, which may be related, respectively, to the mean radius of the free volume cavities and to the relative concentration of holes present in the amorphous regions of the polymer systems. Obviously, τ_3 can be directly correlated to the free volume radius R (Å) by the semiempirical formula:[50]

$$\tau_3 = \frac{1}{\lambda_3} = \frac{1}{2}\left[1 - \frac{R}{R_0} + \frac{1}{2}\sin\left(\frac{2\pi R}{R_0}\right)\right]^{-1} \quad (5)$$

The spherical cavity volume can be calculated by eq 6.

$$V_f = \frac{4}{3}\pi R^3 \quad (6)$$

Panels a and b in Figure 6 show the PALS spectra obtained with the counts (in keV) as a function of energy for the samples S1 and S5. The variation of salt concentration as a function of V_f and τ_3 has been reported by several authors.[47,48] However, the variation of V_f and τ_3 as a function of the composition of plasticized/nanofiller-added polymer electrolytes have hardly been explored.[49,50] Generally, the PALS give three types of lifetime components in polymeric systems. τ_1 relates to para-positronium self-annihilation, whereas τ_2 and τ_3, respectively, relate the free positron and positron/molecular species annihilation and ortho-positronium pick-off annihilation. Each lifetime corresponds to intensity, I_i, which indicates the relative number of annihilations taking place with a particular lifetime. However,

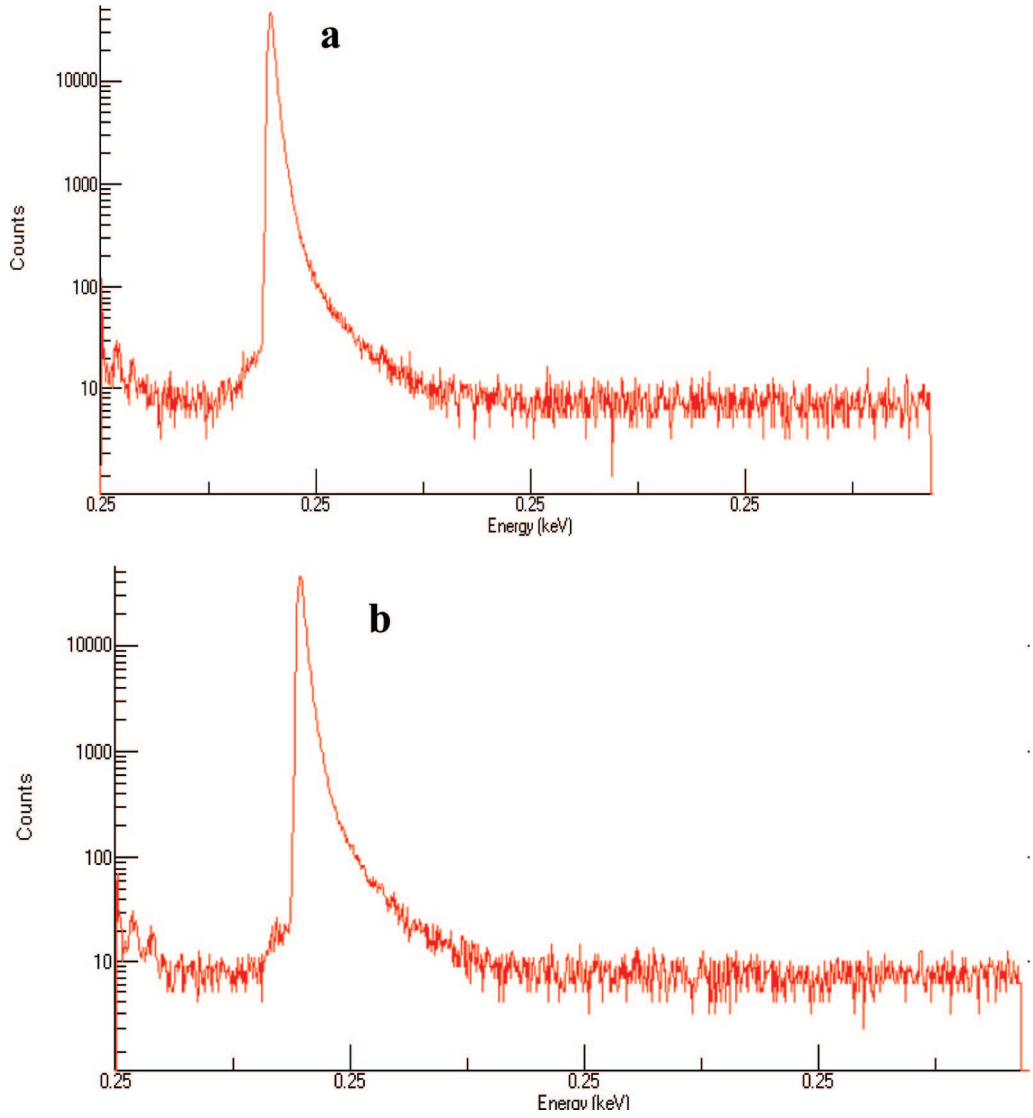

Figure 6. Spectrum for samples (a) S1 and (b) S5 obtained from PALS.

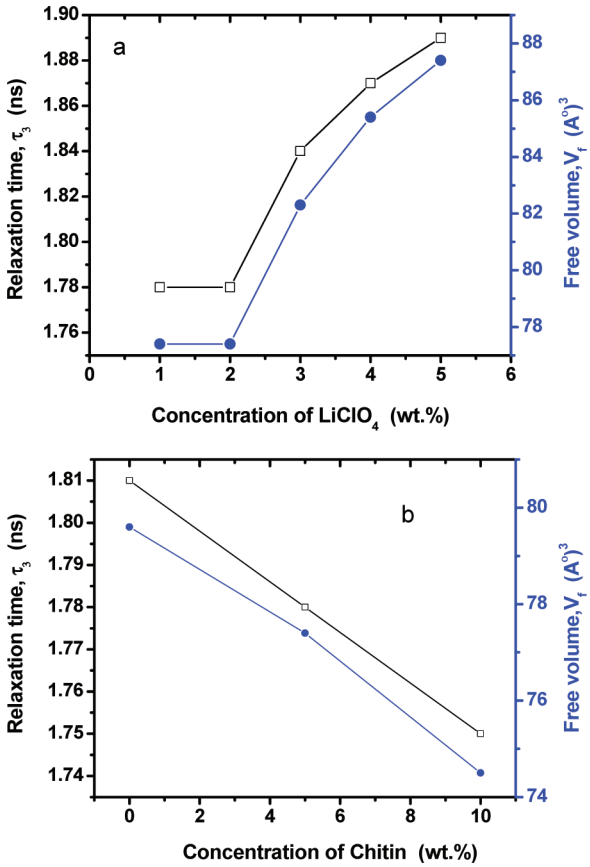

Figure 7. (a) The variation of τ_3 and V_f as a function of lithium salt concentration at 30 °C. (b) The variation of τ_3 and V_f as a function of chitin concentration at 30 °C.

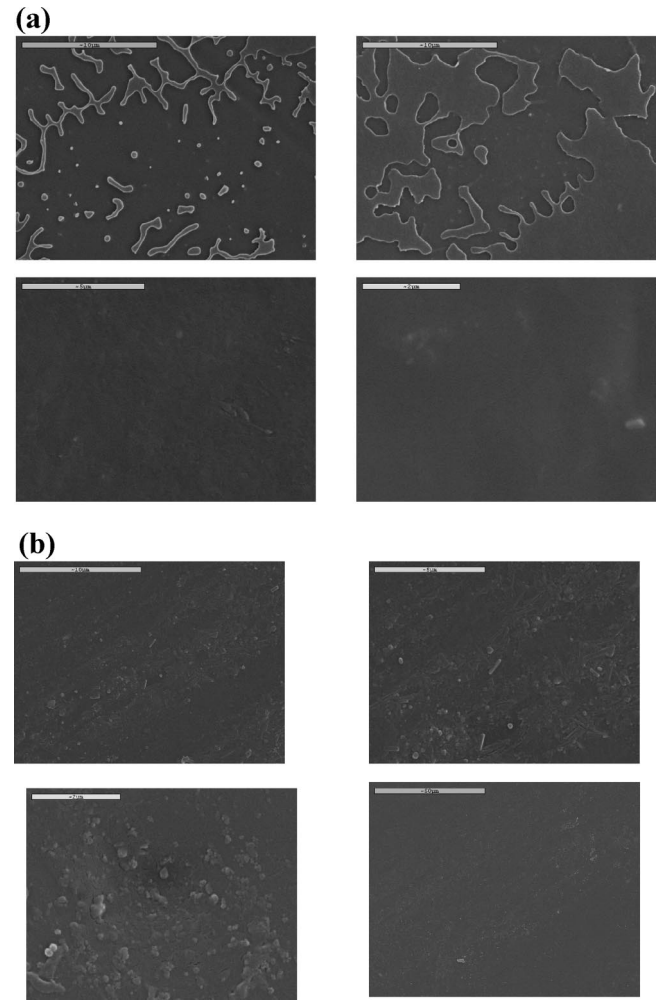

Figure 8. (a) SEM images of PEO + $LiClO_4$ (sample S1). (b) SEM images of PEO + $LiClO_4$ + chitin (sample S5).

for polymeric materials the third component τ_3 with a corresponding I_3 are of great interest due to their dependence on free volume.[51]

Panels a and b in Figure 7 illustrate the variation of orthopositronium lifetime (τ_3), and free volume (V_f) as a function of lithium salt and filler concentration, respectively. The free volume models of plasticizer-added polymeric system shows that addition of low molecular weight plasticizers increases the total volume of the system, resulting in the establishment of the cooperative chain mobility required at the glass transition at lower thermal energies. According to Forsyth et al.,[51] antiplasticization takes place at low concentrations of plasticizers, which reduces the mobility of amorphous chains. This is attributed to the reduction in the mixture of free volume and to a contribution from the absolute free volume of the plasticizer, in this case, tetraglyme. According to Eyring,[52] free volume sites can be classified into two categories, namely, (i) static or interstitial and (ii) dynamic free volumes. The static free volumes remain as holes, which facilitates the flow of polymer chains.

However, dynamic free volume is a time-dependent fraction of the total free volume, and the ratio between the static and dynamic free volumes has been found to be greater than one and also temperature dependent. According to Peng et al.,[47,48] both Li^+ and ClO_4^- ions are unable to promote inhibition or quenching effects, and the observed increase/decrease of the τ_3 or V_f values may be related to the mean radius of free volume cavities that are present in the amorphous phases. It is seen from Figure 7 that the initial addition of filler/salt contributes more toward filler/salt interactions than do plasticizer/polymer interactions. The filler/salt interactions increase the mobility of ions, resulting in an increase in ionic conductivity. The free volume could be increased by filler networking rather than by use of plasticizers. This can also be directly related to an increase of ionic conductivity. We suggest that the network provides an abundance of hopping sites for Li^+ ions in the polymer matrix.[53,54] The enhanced networking leads to an expected increase in the ionic conductivity of the membrane.[54,55] A large increase in the filler content reduces the τ_3 or V_f values (5 wt % of $LiClO_4$) significantly, which may be related to a decrease in the mean radius of the free volume. Such a decrease is attributed to coordination of the Li^+ ions with solvating sites in the polymer.[56] A similar observation has been reported by Fosyrth et al. [51] and Furtado et al.,[57] where the authors probed the lifetime properties of poly(urethane)-based electrolytes by PALS. However, the increase and decrease in the free volume has to be clearly understood.

3.6. SEM Analysis. Panels a and b in Figure 8 show, respectively, typical SEM images of PEO + $LiClO_4$ and PEO + chitin + $LiClO_4$ NCPE membranes. According to Chu et al.,[58,59] the morphology of the electrolyte surface can be modified/tailored by the incorporation of both ionic salts and fillers. The SEM images of PEO + $LiClO_4$ membranes given in Figure 1a shows a smooth surface (5 $LiClO_4$ wt %). SEM images of nanochitin-incorporated membranes (Figure 1b) also show surfaces, which suggest sufficiently good miscibility of nanochitin with the polymer and lithium salt. The smooth morphology is also attributed to a reduction in the crystallinity of PEO due to cross-linking with cations of both lithium ions

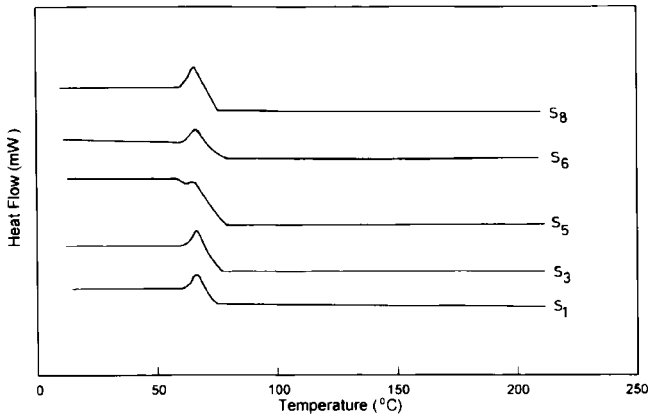

Figure 9. DSC traces of NCPEs.

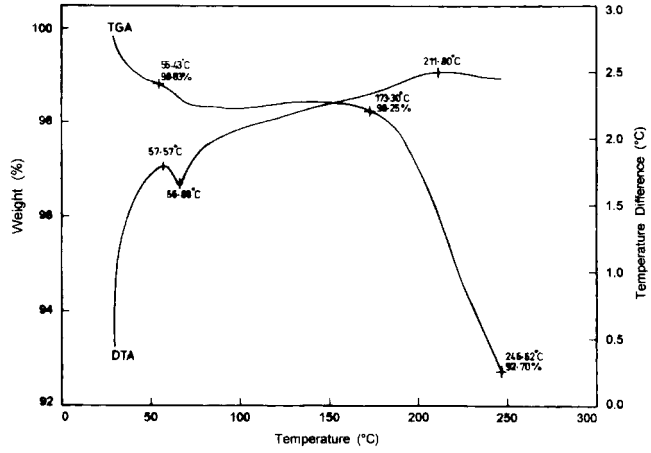

Figure 10. TG-DTA traces of sample S1.

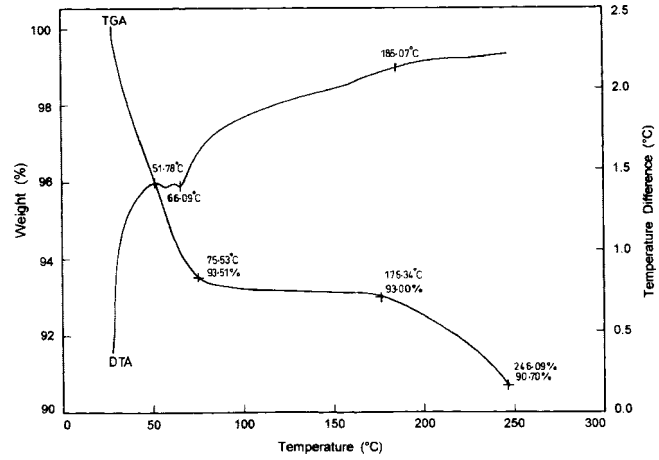

Figure 11. TG-DTA traces of sample S3.

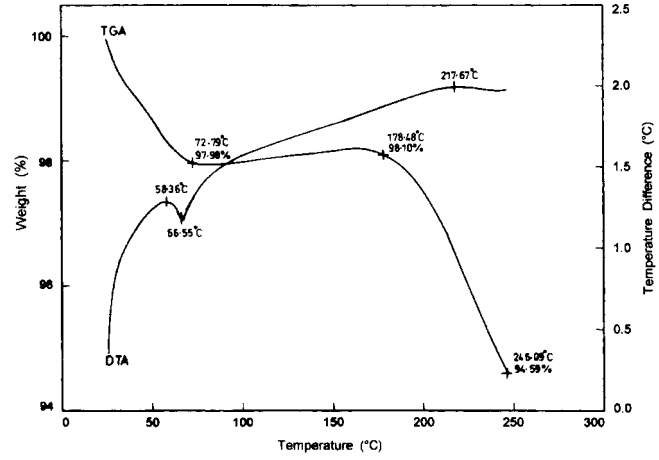

Figure 12. TG-DTA traces of sample S5.

and nanochitin.[60] However, at high contents of nanochitin (about 17 wt %), the membrane is seen to have a rough surface with an inhomogeneous morphology with islands of aggregated particles.

3.7. TG-DTA and DSC Analysis. Figure 9 shows the DSC heating traces of membranes comprising PEO, PEO + $LiClO_4$, and PEO + $LiClO_4$ + nanochitin. The melting endotherm of PEO + $LiClO_4$ (66 °C) gets broadened, and the melting temperature gets reduces as the concentrations of nanochitin and lithium salt are increased. The broadening of the endotherm also takes place with an apparent decrease in the heat of fusion (ΔH_f) with increasing concentration of nanochitin (sample S5).

The TG-DTA traces of PEO + $LiClO_4$ and PEO + $LiClO_4$ + chitin are displayed in Figures 10−12 for the samples S1, S3, and S5, respectively. An endothermic peak observed around 58 °C indicates an eutectic transition of the nanocomposite electrolyte accompanied by a weight loss.[61] The next thermal event occurs beyond 170 °C a region in which the composite electrolyte decomposes.[62] A similar trend can be seen in the TG-DTA traces obtained with nanochitin-incorporated NCPE samples.

4. Conclusions

PEO-based nanocomposite electrolytes with different compositions of chitin and $LiClO_4$ were prepared by a hot press method. Both ionic conductivity and lithium transference number were increased upon the incorporation of chitin in the polymer matrix. Under open-circuit conditions the value of interfacial resistance R_i, has been found be lower for chitin-added samples than for the filler-free sample at 80 °C. Thermal analysis shows that PEO/chitin/$LiClO_4$ electrolytes are thermally stable up to 90 °C. Surface chemistry studies revealed the formation of new compounds on lithium surface which, however, do not make any significant impact on the interfacial resistance of the system. The values of both τ_3 and V_f increase with an increase in salt concentration in the low concentration region, which is attributed to filler/salt interaction. Correlation between the critical free volume and ionic conductivity as a function of temperature and the cycling behavior of $LiFePO_4$/NCPE/Li cells will be published in a future communication.

Acknowledgment. The authors thank Professor A. K. Shukla, Director, Central Electrochemical Research Institute for his interest in this work. The Department of Science and Technology, New Delhi is gratefully acknowledged for financial support through SERC scheme.

References and Notes

(1) Tanaka, T.; Ohta, K.; Arai, N. *J. Power Sources* **2001**, *97*−*98*, 2.
(2) Dell, R. M. *Rand, D.A.J. J. Power Sources* **2001**, *100*, 2.
(3) Tarascon, J.-M.; Armand, M. *Nature* **2001**, *414*, 359.
(4) Zhaghib, K.; Choquette, Y.; Guerti, A.; Simoneau, M.; Belanger, A.; Gautheir, M. *J. Power Sources* **1997**, *68*, 368.
(5) Manuel Stephan, A. *Eur. Polym. J.* **2006**, *41*, 21.
(6) Rhoo, H. J.; Kim, H. T.; Park, J. K.; Huang, T. S. *Electrochim. Acta* **1997**, *42*, 1571.
(7) Appetecchi, G. B.; Croce, F.; Scrosati, B. *Electrochim. Acta* **1995**, *40*, 991.
(8) Song, J. Y.; Wang, Y. Y.; Wan, C. C. *J. Power Sources* **2000**, *77*, 183.
(9) Appetecchi, G. B.; Croce, F.; Persi, L.; Ronci, F.; Scrosati, B. J. *Electrochem. Soc* **2000**, *147*, 4448.

(10) Manuel Stephan, A.; Nahm, K. S. *Polymer* **2006**, *47*, 5952.
(11) Saito, Y.; Kataoka, H.; Manuel Stephan, A. *Macromolecules* **2001**, *34*, 6955.
(12) Manuel Stephan, A.; Muniyandi, N.; Renganthan, N. G.; Karan, R. T. *J. Power Sources* **1999**, *81*−*82*, 751.
(13) Manuel Stephan, A.; Muniyandi, N.; Renganathan, N. G.; Karan, R. T. *Solid State Ionics* **2001**, *130*, 123.
(14) Andrew, Y. G.; Bruce, P. G. *Electrochim. Acta* **2000**, *45*, 1417.
(15) Rinaudo, M. *Prog. Polym. Sci.* **2006**, *31*, 603.
(16) Rudall, K. M.; Kenchington, W. *Biol. Rev.* **1973**, *40*, 597.
(17) Krajewska, B. *Enzyme Microb. Technol.* **2004**, *35*, 126.
(18) Shin, J. H.; Alessandrini, F.; Passerini, S. *J. Electrochem. Soc.* **2005**, *152*, A283.
(19) Appetecchi, G. B.; Hassoun, J.; Scrosati, B.; Croce, F.; Cassel, F.; Salomon, M. *J. Power Sources* **2003**, *124*, 246.
(20) Evans, J.; Vincent, C. A.; Bruce, P. G. *Polymer* **1987**, *28*, 2324.
(21) Heo, Y.; Kang, Y.; Han, K.; Lee, C. *Electrochim. Acta* **2004**, *50*, 345.
(22) Chusid, O.; Gofer, O.; Aurbach, Y.; Watanabe, D.; Momma, M.; Osaka,T., T. *J. Power Sources* **2001**, *97*, 98–632.
(23) Robitailla, C. D.; Fauteux, D. *J. Electochem. Soc.* **1986**, *133*, 133–315.
(24) Capiglia, C.; Mustarelli, P.; Quartarone, E.; Tomasi, C.; Magistris, A. *Solid State Ionics* **1999**, *118*, 73.
(25) Vilano, P.; Carewska, M.; Appetecchi, G. B.; Passerini, S. *J. Electrochem. Soc.* **2002**, *149*, A1282.
(26) Wieczorek, W.; Florjancyk, Z.; Stevens, J. R. *Electrochim. Acta* **1995**, *40*, 2251.
(27) Przluski, J.; Siekierski, M.; Wieczorek, W. *Electrochim. Acta* **1995**, *40*, 2101.
(28) Croce, F.; Curini, R.; Martinelli, A.; Persi, L.; Ronci, F.; Scrosati, B.; Caminiti, R. *J. Phys. Chem. B* **1999**, *103*, 10632.
(29) Croce, F.; Persi, L.; Scrosati, B.; Flory, F. S.; Plichta, E.; Hendrikson, M. A. *Electrochim. Acta* **2001**, *46*, 2457.
(30) Li, Q.; Takeda, Y.; Imanish, N.; Yang, J.; Sun, Y. K. *J. Power Sources* **2001**, *97*−*98*, 795.
(31) Li, Q.; Imanishi, N.; Hirano, A.; Takeda, Y.; Yamamoto, O. *J. Power Sources* **2002**, *110*, 38.
(32) Li, Q.; Itoh, T.; Imanishi, N.; Hirano, A.; Takeda, Y.; Yamamoto, O. *Solid State Ionics* **2003**, *159*, 97.
(33) Ismail, I.; Noda, A.; Nishimoto, A.; Watanabe, M. *Electrochim. Acta* **2001**, *46*, 1595.
(34) Owen, J. R. *Br. Polym. J* **1988**, *4*, 227.
(35) Oleksiak, A. L. *Solid State Ionics* **1999**, *119*, 205.
(36) Sloop, S. E.; Lerner, M. M. *J. Electrochem. Soc.* **1996**, *143*, 1292.
(37) Silverstein, S. M. ; Bassler,C. ; Morrill,C. ; *Spectrometric Identification of Organic Compounds*; John Wiley & Sons: 1996.
(38) Rocco, A. M.; Moreira, D. P. *Eur. Polym. J.* **2003**, *95*, 1925.
(39) Silverstein, R. M.; Webster, F. X. *Electrochim. Acta* **1995**, *40*, 2333.
(40) Chartoff, P.; Lo Thomas, S. K.; Harrell, E.; Roc, R. J. *Macromol. Sci. Phys. B* **1981**, *20*, 287.
(41) Pearson, F. G.; Marchessault, R. H.; Liang, C. Y. *J. Polym. Sci.* **1960**, *13*, 101.
(42) Focher, B.; Naggi, A.; Torri, G.; Cosari, A; Terbjerich, M. *Carbohydr. Polym.* **1992**, *17*, 97.
(43) Ramesh, S.; Yuen, T. F.; Shen, C. J. *Spectrochim. Acta A* **2008**, *69*, 670.
(44) Hodge, R. M.; Bastow, T. J.; Edward, G. H.; Simon, G. P.; Hills, A. J. *Macromolecules* **1996**, *29*, 8137.
(45) Wang, C. L.; Maurer, F. H. *Macromolecules* **1996**, *29*, 8249.
(46) Jean, Y. C. *Microchem. J* **1990**, *42*, 72.
(47) Peng, Z. L.; Wang, B.; Li, S. Q.; Wang, S. J.; Liu, H.; Xie, H. *Phys. Lett.A.* **1994**, *194*, 228.
(48) Peng, Z. L.; Wang, B.; Li, S. Q.; Wang, S. J. *J. Appl. Phys.* **1995**, *334*, 7711.
(49) Elwell, R. J.; Pethrick, R. A. *Eur. Polym. J.* **1990**, *26*, 853.
(50) Okada, T.; Nishijima, S.; Honda, Y.; Kobayashi, Y. *J. Phys. IV* , *C4* (3), 291.
(51) Forsyth, M.; Meakin, P.; MacFarlane, D. R.; Hill, A. J. *J. Phys.: Condens. Matter* **1995**, *7*, 7601.
(52) Eyring, H. *Chem. Phys.* **1936**, *4*, 28.
(53) Belgacem, M. N.; Blayo, A.; Gandini, A. *J. Colloid Interface Sci.* **1996**, *182*, 431.
(54) Nair, K. G.; Dufresne, A. *Biomacromolecules* **2003**, *4*, 657.
(55) Nair, K. G.; Dufresne, A. *Biomacromolecules* **2003**, *4*, 1835.
(56) Hill, A. J.; Zipper, M. D.; Tant, M. R.; Stack, G. M.; Jordan, T. C.; Shultz, A. R. *J. Phys.: Condens. Matter.* **1996**, *8*, 3811.
(57) Furtado, C. A.; Silva, G. G.; Machado, J. C.; Pimenta, M. A.; Silva, R. A. *J. Phys. Chem. B* **1999**, *103*, 7102.
(58) Schechter, A.; Aurbach, D. *Langmuir* **1999**, *15*, 3334.
(59) Chu, P. P.; Reddy, M. J.; Kao, H. M. *Solid State Ionics* **2003**, *156*, 141.
(60) Chiang, C. Y.; Reddy, M. J.; Chu, P. P. *Solid State Ionics* **2004**, *175*, 631.
(61) Ribeiro, R.; Silva, G. G.; Mohallen, N. D. S. *Electrochim. Acta* **2001**, *46*, 1679.
(62) Shodai, T.; Owens, B. B.; Ostsuka, M.; Yamaki, J. *J. Electrochem. Soc.* **1994**, *141*, 2978.

JP808640J